Direct Simulation of Turbulent Particle Transport in Electrostatic Precipitators

Alfredo Soldati, Paolo Andreussi, and Sanjoy Banerjee

Dept. of Chemical and Nuclear Engineering, University of California, Santa Barbara, CA 93106

The dispersion of particles in turbulent duct flow under the influence of electrostatic fields is studied using direct numerical simulation. In this new approach, particles are moved in the temporally and spatially varying turbulent flow field under the influence of electrostatic and gravitational body forces, as well as fluid dynamic drag. The simulations agree well with previously performed experiments (done in geometries typical of wire-plate and plate-plate electrostatic precipitators) not only in the overall collection efficiency of particles, but in particle concentration profiles at various axial locations in the flow direction. This gives confidence in the technique that may be used to study different precipitator geometries and flow field configurations, supplementing costly and difficult experiments. Furthermore, information is obtained at a much more detailed level than is possible via experiments, allowing insights into the mechanisms dominating particle collection.

Introduction

In electrostatic precipitators (ESPs) airborne particles are driven toward collecting electrodes by the effect of an applied electrostatic field. The particles are usually charged in the region close to the entrance of a precipitator by ions released from an electrode. Due to the complex interactions between the usually turbulent flow field, the particles and the electrostatic field, the phenomena involved in the electrostatic precipitation are not yet clearly understood. The complexity arises because the motion of particles transported by the gas stream is determined by both body forces and flow field, which is turbulent. Each of these may be influenced by other factors; for example, the flow field may interact with the electrostatic field if there is corona discharge, and similarly, the motion of charged particles may modify the electrostatic field. The most important of these complicative factors appear to be discharge-related phenomena that give rise to the effect called *Corona Wind* (Yamamoto and Velkoff, 1981; Leonard et al., 1983; Castellanos, 1991; Kallio and Stock, 1992; McCluskey and Perez, 1992) comprising streams of fast ions that move across the duct. Indeed, the substantial momentum released by the

ions to the fluid molecules can induce secondary turbulence patterns that may affect particle transport and deposition.

Recent emphasis on particulate emission control has led to a renewed interest in electrostatic precipitation. In earlier works, the prediction of particle transport in ESPs has been achieved by the solution of simplified convection/diffusion equations. The problem usually relates to the modeling of the diffusion coefficient in an interacting turbulent field-electrostatic field. Pioneering work by Deutsch (1922) supposed turbulent mixing to be effective enough to maintain the cross-stream concentration profile uniform along the precipitator duct. Deutsch's assumption still constitutes the basis for industrial design of ESPs. An analytical solution of the two-dimensional convection/diffusion equation presented later by Leonard et al. (1980) was expressed in terms of a dimensionless number based on a uniform diffusion coefficient. Essentially, the same equation was numerically solved by Williams and Jackson (1962) and more recently by Kihm (1987). Kihm considered nonuniformities in the diffusion coefficient, assigning it different values in the wall region (low diffusion) and in the central region (high diffusion) of the channel.

On the experimental side, successful attempts to measure particle transport in turbulent fields with electrostatic body forces were reported, for instance, by Yamamoto and Velkoff (1981), Leonard (1982), Kihm (1987), and Kallio (1987). The
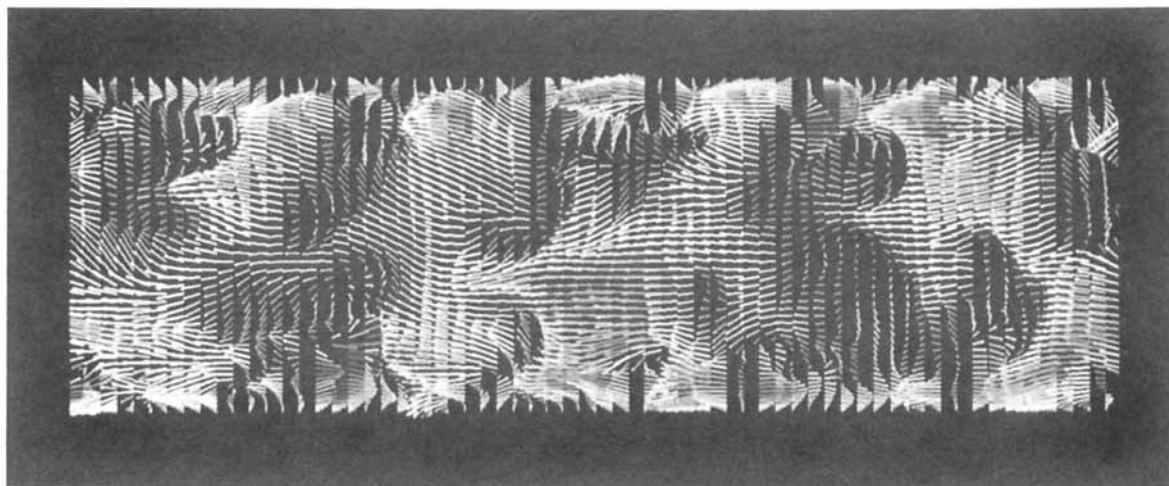
Figure 1. Instantaneous (also fluctuating) velocity vectors in a *y-z* plane.

y is the vertical and wall parallel direction, and *z* is the wall normal. Magnitude of vectors is the modulus of the fluctuating velocity in the *y-z* plane. Brightness of vectors (light denotes high, dark denotes low) is the intensity of the streamwise (*x*, well parallel horizontal) fluctuating velocity.

experiments documented by Kihm (1987) and Self et al. (1987) are particularly interesting, since they address particle transport in plate-plate and wire-plate precipitators considering both cases with and without ionic discharge. These experimental results are used by Kihm (1987) in the numerical solution of the convection/diffusion equation through the use of a spatially varying diffusion coefficient.

However, even at the low values of the Reynolds number, typical of electrostatic precipitators, the flow in the duct is fully turbulent and turbulence is a completely three-dimensional phenomenon with motions from scales characteristic of the duct dimensions down to scale typical of viscous dissipation (orders of magnitude smaller). Hence, transport characteristics are local and cannot easily be described through the use of averaged equations. As an example, Figure 1 shows an instantaneous cross section of a turbulent channel flow that has been simulated. The intricacy of the fluid motion is evident. Such a complete resolution of the turbulent flow field allows the calculation of particle transport without any need of tunable parameters. As will be discussed later, particles are moved at every instant by such a changing flow field and body forces. Since the flow field is fully resolved in DNS, there is no need for diffusion coefficients as postulated in all previous work.

To completely resolve the turbulent flow field in an electrostatic precipitator, the Navier-Stokes equations are solved by a pseudo-spectral technique. Details are presented later. Earlier work (Kim et al., 1987; Lam and Banerjee, 1992) demonstrated that this technique resolves all the meaningful scales of the turbulence for Reynolds numbers in the range typical of ESPs. In the cases analyzed here, the transport of particles immersed in a turbulent flow field and under the action of different stationary electrostatic fields are examined.

Two different configurations of precipitators, as shown in Figure 2, have been chosen: plate plate and wire plate. The plate-plate precipitator can be considered as the second stage of a two-stage precipitator, the first stage being a section where particles are charged. The precharged aerosol particles suspended in the main gas stream enter the duct, and the electric field is then kept constant and uniform throughout the pre-

cipitator. A potential difference is maintained between the plates to drive particles toward the collecting electrode.

The wire-plate precipitator is a one-stage precipitator, since particles are charged and separated from the main stream of the flow in the same stage. The charging is done by ionic discharge mainly from the wires near the entrance. In this article, no discharge that could couple the electrostatic field and the turbulent field is considered. This is a necessary first step in investigating the effect of turbulence on precipitator behavior. The effect of coupling between fields will be discussed in a later publication.

Computational Methodology

Particle transport in a pressure-driven turbulent flow bounded by flat walls is discussed here. The fluid is incompressible, Newtonian and the particle concentration is so low that the particles do not affect the flow. As discussed previously, the coupling between the electrostatic and fluid field is also absent for the cases studied. Therefore, the fluid dynamic field has been calculated for a sufficiently long time interval, and it is the same for the two configurations analyzed. In the wire-plate configuration, the wake that might have been produced by the wires is also neglected, since the turbulence level in the channel center is believed not to be significantly influenced. It should be emphasized that the fluid velocity field so generated is fully three-dimensional, time-varying, and resolved down to the finest scales of motion.

Fluid dynamic field

The dimensionless momentum balance equations for the fluid are:

$$\frac{\partial u_i}{\partial t} = -u_j \frac{\partial u_i}{\partial x_j} + \delta_{3i} + \frac{1}{Re} \frac{\partial^2 u_i}{\partial x_i^2} - \frac{\partial p}{\partial x_i} \tag{1}$$

where δ_{3i} is the mean kinematic pressure gradient that drives
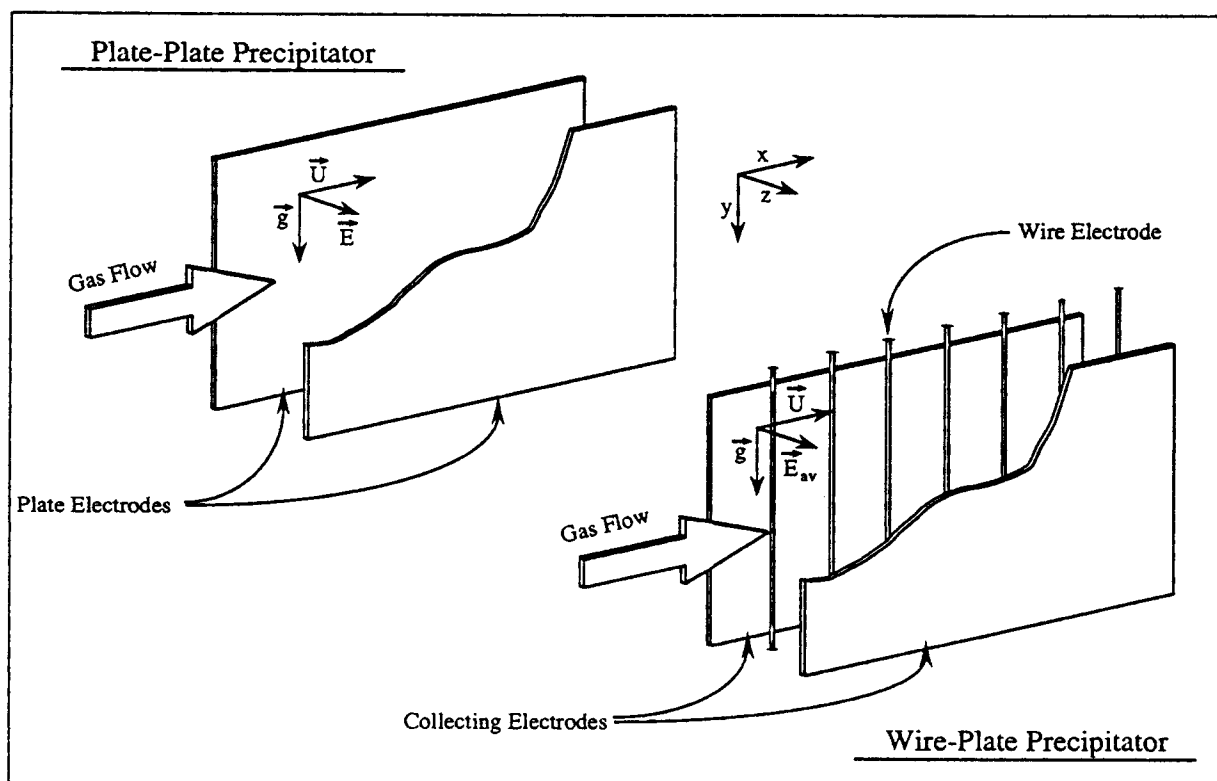
Figure 2. Plate-plate and wire-plate precipitator geometries.

the flow. Equation 1 was made dimensionless using the duct half-spacing, h, and the shear velocity, u_τ, defined as:

$$u_\tau = \sqrt{\frac{\tau_w}{\rho_f}} \qquad (2)$$

where τ_w is the shear at the wall and ρ_f is the fluid density. Equation 1 is solved by taking the curl twice. A Helmholtz-type equation of the fourth order in the velocity is obtained. A pseudospectral method is used to calculate the solution of the flow field. At both walls, conditions of no-slip are applied, while periodic boundary conditions are used in the streamwise and spanwise (or vertical) directions. To represent the solution, finite Fourier expansions are adopted in the streamwise and spanwise (wall parallel) directions; to deal with the finiteness of the domain, Tchebychev polynomials are used in the cross-stream (wall normal) direction. The velocity field is then expanded in the form:

$$u(x,y,z)$$
$$= \sum_{k_1} \sum_{k_2} \sum_{k_3} \hat{u}(k_1,\, k_2,\, k_3) e^{i(k_1 x + k_2 y)} \cos(k_3 \cos^{-1} z) \qquad (3)$$

where $\hat{u}(k_1,\, k_2,\, k_3)$ represents the velocity field in the phase space, k_1 and k_2 are wavenumbers in the streamwise and vertical directions, and k_3 is the wavenumber in the wall-normal direction.

The adoption of the Fourier-Tchebychev expansions makes the calculation algorithm very accurate. However, calculating the products involved in the convection term (first term in the righthand side of Eq. 1) would require a time-consuming convolution integral. Therefore, through the use of the fast Fourier transform, products are calculated in the physical space and the results are backtransformed into wave number space, giving rise to the name pseudospectral.

Time advancement is provided by a two-level Adams-Bashforth method for the convective terms and by an implicit Crank-Nicolson method for the diffusive terms. This numerical technique has been implemented in the code described in detail by Lam (1989) and Lam and Banerjee (1992). To run the present simulations, modifications have been made to that code to cope with different boundary conditions and to improve the efficiency of the code itself.

The dimensions of the computational domain are $4\pi h \times 2\pi h \times 2h$. This size was chosen large enough to justify the application of periodic boundary conditions in the streamwise and spanwise directions. Indeed, the choice of the dimensions was guided by previous measurements of Comte-Bellot (1963), indicating that spatial correlations in the streamwise direction become negligible at a distance of approximately $3.6h$. In the spanwise direction, spatial correlations become negligible at a distance of about $1.6h$, roughly half the characteristic streamwise correlation distance (Utami and Ueno, 1987). A-*posteriori* analyses of the calculations proved the dimensional choice to be suitable for the problem analyzed.

Electrostatic field

In the plate-plate precipitator, the electrostatic field is uniform and constant. On the other hand, in the wire-plate case, the electrostatic field, although constant, is highly nonuniform

and calculated solving the following reduced set of Maxwell equations:

$$\frac{\partial^2 V}{\partial x_i^2} = 0 \tag{4}$$

$$E_i = \frac{\partial V}{\partial x_i} \tag{5}$$

where V and E are the electrostatic potential and the electrostatic field, respectively. The system is solved for the particular geometry of the wire-plate precipitator adopting the image charge technique (Bohm, 1970). The two-dimensional electrostatic field components, E_x along the streamwise direction and E_z along the wall normal direction, have the following form:

$$E_x = \frac{\pi V_c}{2hF} X_x \quad E_z = \frac{\pi V_c}{2hF} X_z \tag{6}$$

where V_c is the electric potential applied to the wire electrodes, F is the form factor, and X_x and X_z are the field shape factors. The expression for these factors is reported in the Appendix.

To compare the results of the two different precipitator configurations, the value of the average electrostatic field, E_{av}, was maintained for the two cases at $240 \text{ kV} \cdot \text{m}^{-1}$. For the wire-plate case this value was obtained applying a voltage of 12 kV at each of the wire electrodes, whereas for the plate-plate case a potential difference of 9.6 kV was maintained between the plate electrodes.

Particle dynamics

To simulate dispersion, particles in number sufficiently large to have reasonably meaningful statistics were homogeneously dispersed in the turbulent duct flow. A random number generator was used to randomly distribute particles in the whole domain. Particle trajectories have been followed individually by numerically solving the equation of motion (Maxey and Riley, 1983). Terms included in the particle motion equation are the electrostatic body force, the gravity force, and the fluid dynamic drag. Other forces, such as the Basset history force, the Saffman lift force, the Magnus effect, the hydrostatic force, and the added mass force, are assumed to be negligible for the case treated (Maxey and Riley, 1983). In fact, calculations showed that these effects are orders of magnitude less important than the three forces considered in the equation. It has been hypothesized further that particles are rigid and pointwise, and at a concentration low enough to make particle-particle interactions, due to either inertial force or electrostatic repulsion force, it is negligible.

The vectorial equation of motion, made dimensionless using scales characteristic of the wall region, that is, the shear velocity u_τ and the fluid kinematic viscosity v_f, is:

$$\frac{dv}{dt} = -\frac{v - u}{\tau_p} + g + \frac{1}{Fr_p^2} e \tag{7}$$

The equation has been integrated with an explicit method for each single particle, where particle and fluid velocities are u and v, τ_p is the particle relaxation time, g is the gravity vector,

and e is the electric field unity vector. The particle relaxation time, τ_p, measuring the particle responsiveness to a change in fluid velocity, can be written as:

$$\tau_p = \frac{d_p^2 \rho_p}{18 \mu_f} \frac{1}{1 + 0.15 Re_p^{.697}} \tag{8}$$

where Re_p is the particle Reynolds number based on the particle velocity relative to the fluid velocity, on the particle diameter, d_p and on the fluid kinematic viscosity, v_f. The expression for the fluid dynamic drag force used in this equation is the one proposed by Rowe and Henwood (1962).

In Eq. 7, the dimensionless electric-Froude number, Fr_p, represents the square root of the ratio of the inertial force to the electrostatic force acting on the particle and it has the following form:

$$Fr_p^2 = \frac{m_p u_\tau^3}{q_p v_f E} \tag{9}$$

where m_p and q_p are particle mass and particle charge, respectively, and E is the electrostatic field modulus. A measure of the strength with which a particle drifts toward the collector is given by the migration velocity, w_e. The migration velocity is a reference velocity calculated by balancing the drag force and the Coulomb force acting on the particle. It has the following expression for Stokes drag ($Re_p < 1$):

$$w_e(x, y, z) = \frac{q_p E(x, y, z)}{3 \pi d_p \mu_f} \tag{10}$$

In both simulated cases, if the average electrostatic field were considered, the average migration velocity is about 5.05 $\text{cm} \cdot \text{s}^{-1}$ directed toward the collecting electrodes.

Results and Discussion

Experiment

In industrial applications, the evaluation of the concentration of particles is still based on a Deutsch-type equation, leaving to some correction coefficient the responsibility for taking care of the inadequacy arising from such a description (Robinson, 1967; Riehle and Löffler, 1992). The Deutsch equation assumes an exponential decay law for particle concentration in the following form:

$$n(De) = n_0 e^{-De} \tag{11}$$

where n is the particle number, n_0 is the particle number at the inlet section, and De, the Deutsch number, represents the dimensionless length covered by particles and has the form:

$$De = \frac{w_e x}{U_m d} \tag{12}$$

where d is the characteristic width of the precipitator, U_m is the mean flow velocity, and x is the streamwise coordinate. The fractional efficiency is then defined as:

$$\eta(De) = 1 - e^{-De} \tag{13}$$

Table 1. Parameters of the Simulation

Reynolds number:	$Re_{Dh} = (U_m D_h)/\nu_f = 6{,}000.0$
Shear Reynolds number:	$Re_\tau = u_\tau h/\nu_f = 108.0$
Dimensionless mean velocity:	$U_m/u_\tau = 13.7$
Mean velocity:	$U_m = 1.16 \text{ m} \cdot \text{s}^{-1}$
Centerline velocity	$U_c = 1.40 \text{ m} \cdot \text{s}^{-1}$
Fluid viscosity:	$\nu_f = 15.7 \; 10^{-6} \text{ m}^2 \cdot \text{s}^{-1}$
Fourier modes (x):	$N_x = 64$
Fourier modes (y):	$N_y = 64$
Tchebychev modes (z):	$N_z = 65$
Time step:	$Dt_\tau = Dt(u_\tau/h) = 0.001$
Total number of aerosol particles:	$N_p = 4{,}000$
Particle diameter:	$d_p = 4.0 \; \mu\text{m}$
Aerosol density:	$\rho_p = 898.0 \text{ kg} \cdot \text{m}^{-3}$
Average electric field:	$E_{av} = 240.0 \text{ kV} \cdot \text{m}^{-1}$
Number of wires (wire-plate case):	$n_w = 7$
Applied voltage (wire-plate case):	$V_c = 12.0 \text{ kV}$
Wire electrode radius:	$r_c = 0.445 \; 10^{-3} \text{ m}$

Figure 4. Reynolds stress ($u' w'$).

Comparison of computed results (——) and experimental data (o) by Eckelmann.

This exponential decay law greatly underestimates the efficiency in experimental facilities. Of course, in industrial facilities, a number of other effects become important, for example, high-resistivity dust piling up on plates and back corona discharge.

To validate the simulation, experimental results including no electrohydrodynamic coupling between electrostatic and flow field obtained by Kihm (1987) have been considered first. The experiments cover both plate-plate and wire-plate precipitator configurations for different flow parameters and particle migration velocity, and they were performed to examine the effects of turbulent diffusion on electrostatic precipitator performance. Therefore, the experiments were performed for different flow conditions having both boundary generated turbulence and using baffles to trip the flow. The experimental duct was 5 cm wide, and measurements were made at 20 and 40 cm downstream of the inlet section (the inlet section is defined by the upstream boundary of the electrostatic field). When baffles were employed, they were put 40 cm before the inlet section. In the case of 1-cm-wide baffles, flow conditions after 40 baffle widths are already rather independent of baffle presence. The presence of baffles actually serves to trip the laminar boundary layer into a turbulent one. Kihm (1987) presents the streamwise turbulence intensity profiles, measured with the hot-wire technique. It is evident that roughly 80 baffle widths downstream the baffle location, in correspondence with the second meas-
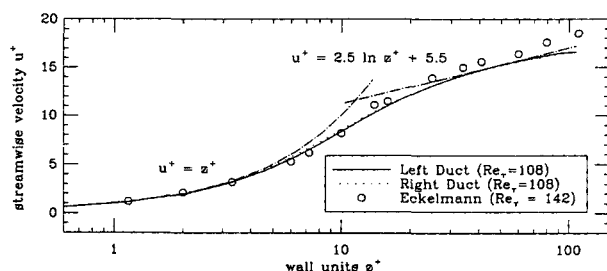
uring section, the intensity profiles are completely independent of baffle presence and typical of wall turbulence.

Other sets of experimental data were obtained using different baffles: larger baffles (2 cm) and double baffles. In the case of larger baffles, the turbulence intensity profiles are strongly influenced far downstream of the inlet section so that no comparison with the present results is advisable. In the case of double baffles, typical duct turbulence profiles are again recovered in the measuring sections.

Fluid dynamic field

The simulation was performed in both plate-plate and wire-plate cases by first obtaining a turbulent flow field in a duct and then homogeneously distributing 4,000 precharged particles throughout the whole domain. Particles have been followed until the majority of them were collected. The fluid is air, and particles are 4-μm-dia. aerosol droplets. Table 1 shows parameters relative to the simulation.

To achieve stationary turbulence, the code has been run for about six dimensionless time units, corresponding to 6,000 time steps, when the total shear stress became linear and steady, thus indicating sufficiently long time for good statistics for the flow field. Then, some six dimensionless time units more have been run to generate the database necessary to carry out turbulence statistics and to constitute a suitable data field to simulate particle transport.

To assess the validity of the simulation, turbulence statistics have been compared against experimental data. Figures 3 and 4 show the mean velocity profile (in semilogarithmic plot) and the Reynolds stress component $<u' w'>$ against data of Eckelmann (1974) with an oil channel. The Reynolds stress com-

Figure 3. Mean streamwise velocity.

Comparison of computed results or the right part (——) and left part (-•-•) of the channel, experimental data (o) by Eckelmann and correlation from literature (- - - -).
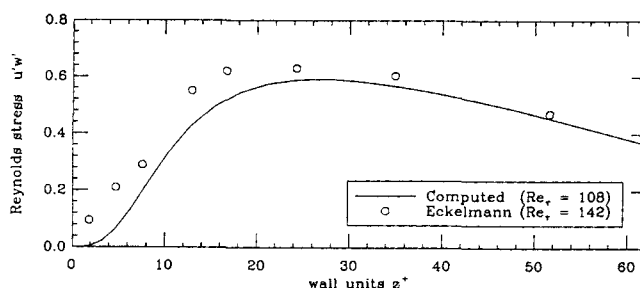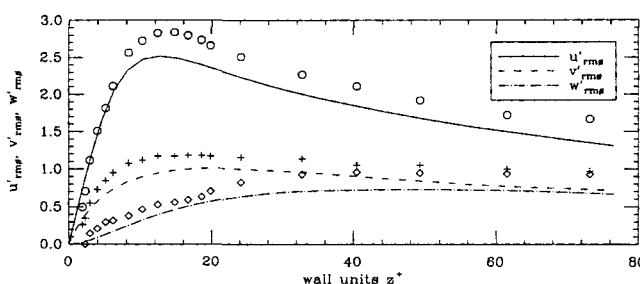

Figure 5. Turbulence intensities in x, y, and z directions.

Comparison of computed results (——) and experimental data (o) by Kreplin and Eckelmann.
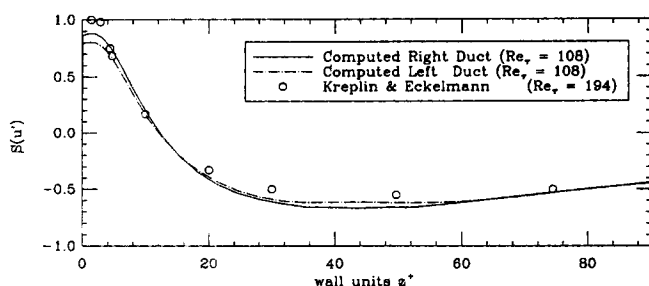
Figure 6. Skewness of the streamwise fluctuating velocity.

Comparison of computed results for the right part (——) and left part (-·-·-) of the channel against experimental data (o) by Kreplin and Eckelmann.

Figure 8. Plate-plate precipitator.

Trajectory (⊖) of a particle, its velocity (——) and fluid velocity at particle location. The particle starts from the middle of the channel and deposits at the wall.

ponent is defined here as the product of the fluctuating components of the velocity u' and w'. The agreement is very good, qualitatively and quantitatively, although the data have slightly larger values than the computed results. Since data were obtained for $Re_\tau = 142$ while the computation is for $Re_\tau = 108$, the small discrepancy is probably due to a Reynolds effect number, as discussed by Antonia et al. (1992). However, Kim et al. (1987), referring to the studies by Eckelmann and Kreplin (1979), Wallace et al. (1972), and Brodkey et al. (1974), argue that proper u_τ has to be used as scaling velocity and the data by Eckelmann (1974) have to be divided by a coefficient of 1.06 to improve the comparison. In this work, data are presented as originally published. Figure 3 also shows the linear law of the wall and the logarithmic law for the outer region of the channel and the agreement is better than satisfactory. The logarithmic law was plotted using well assessed coefficients from the literature (Tennekes and Lumley, 1972). Figure 5 compares turbulence intensities against the data by Kreplin and Eckelmann (1979) obtained for $Re_\tau = 194$. The higher values shown by the data are very likely due to the effect of the shear Reynolds number and perhaps the effect indicated by Kim et al. (1987). For the velocity component in the streamwise direction, the third- and fourth-order moments, the skewness and flatness, respectively, are also presented in Figures 6 and 7 and compared with the data by Kreplin and Eckelmann (1979). The skewness is a measure of the asymmetry of the fluctuation distribution, and the flatness indicates whether or not the values of the function are high close to the edges of
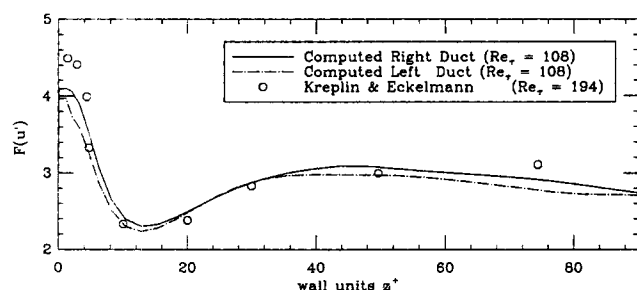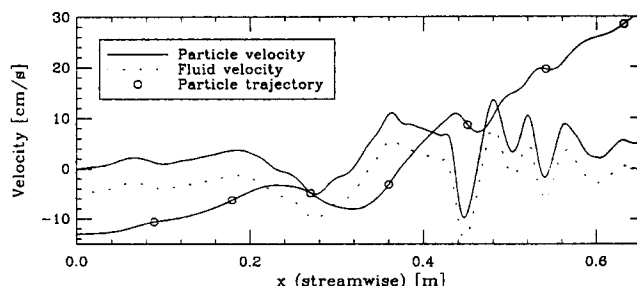
the domain. The agreement with the experiments is very good also for these higher-order statistics.

Particle transport in plate-plate geometry

Given the characteristics of the technique for performing the simulations, individual particle positions could be monitored at each timestep. Therefore, trajectories, concentration profiles, and efficiency of the precipitator could have been plotted for all the values of the Deutsch number. To show the capabilities of the simulation, Figure 8 shows the trajectory of a particle and its velocity, and the fluid velocity at particle location. The particle path is in arbitrary units, while velocities are in $cm \cdot s^{-1}$. The particle is initially located in the middle of the duct and eventually it deposits on the wall. There is a roughly constant shift between the fluid velocity and the particle velocity, due to the electrostatic drift. However, the relative velocity is not really constant. The particle relaxation time being very small, the particle follows turbulent fluctuations rather closely. Figure 9 shows the fractional concentrations for different downstream locations. It is noted that profiles are well developed showing that turbulent diffusion plays a significant role in the deposition process. If the flow were laminar, particles would be transported toward the collecting plate with no deviations, and concentration profiles would look like sharp steps. In the other extreme case, if turbulent diffusion were infinitely effective, as in Deutsch's assumption, concentration profiles would look uniform throughout the whole duct.

A comparison of experimental results in Figure 10 is for the same Deutsch number and experiments are by Kihm (1987) for
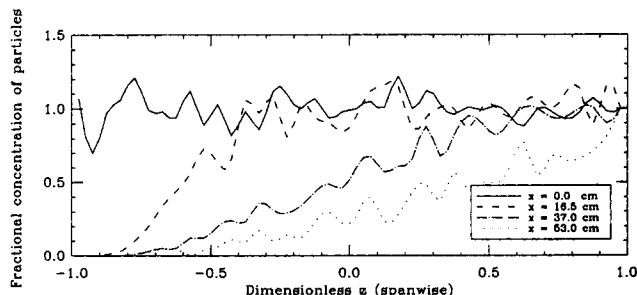

Figure 7. Flatness of the streamwise fluctuating velocity.

Comparison of computed results for the right part (——) and left part (-·-·-) of the channel against experimental data (o) by Kreplin and Eckelmann.

Figure 9. Plate-plate precipitator.

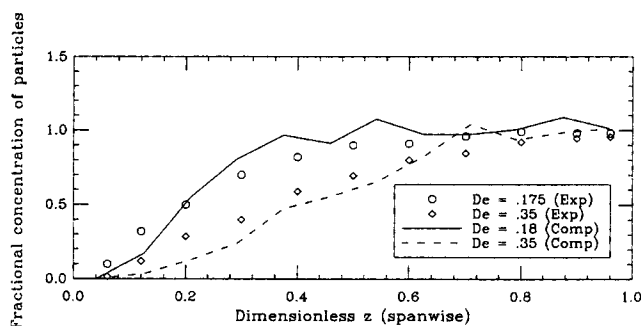Evolution of particle fractional concentration profiles along the streamwise coordinate.

Figure 10. Plate-plate precipitator.

Particle fractional concentration at two different dimensionless coordinates (Deutsch numbers). Comparison of computed results (——, - - - -) against data by Kihm (o , ◊).

a mean velocity of $2 \text{ m} \cdot \text{s}^{-1}$ and for 1-cm baffles. The agreement is excellent both quantitatively and qualitatively. In fact, the shape of concentration profiles matches the experimental data very well, indicating the power of the simulating technique. Efficiencies were also computed and compared with experimentally obtained ones for a range of Deutsch numbers. In Figure 11, efficiencies are compared on a semilogarithmic plot with the solid line representing the Deutsch equation (Eq. 13). The same data are presented in Table 2. It is worth noting that both experimental data and numerical results, which agree well, are well above the Deutsch efficiency line.

Particle transport in wire-plate geometry

In the wire-plate geometry, the electrostatic field is constant, but not uniform, having maxima at wires locations, and it has the same average intensity as in the plate-plate case. Hence, the average migration velocity of particles is also the same. Due to the complex distribution of the electrostatic field, however, the electrostatic body force that acts on a particle changes depending on particle position. The electrostatic field has a strong influence in the wire region, whereas turbulent transport is dominant in the wall region. In fact, turbulence intensity is maximum in the wall region, where electrostatic forces are weaker.
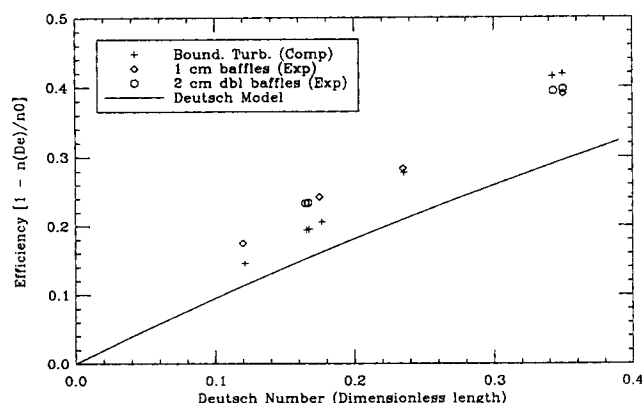
Table 2. Plate-Plate Precipitator Efficiencies

Deutsch No.	Deutsch Eff.	Exp.	Comp.
0.120	0.113	0.175*	0.146
0.165	0.152	0.233**	0.194
0.167	0.154	0.234**	0.195
0.175	0.160	0.242*	0.205
0.235	0.209	0.284*	0.278
0.343	0.290	0.394**	0.410
0.350	0.295	0.397**	0.420
0.350	0.295	0.389*	0.420

* 1-cm single baffles
** double baffles

A plot of a particle trajectory and velocity, and fluid velocity at the particle positions is shown in Figure 12. Initially, the particle was located at the duct centerline and at the end of its trajectory it deposits. The dimensions of the velocity are in $\text{cm} \cdot \text{s}^{-1}$, while the particle path is in arbitrary units. Particle relaxation time is very small so that without electrostatic drift particles would have virtually no lag following the flow. On the average, the electrostatic drift velocity again gives the particle a roughly constant velocity lag. However, in contrast to the plate-plate case, close to the wire region, electrostatic field effects are quite noticeable through the presence of peaks in the velocity plot corresponding to the wire locations. In this case, although the average value of the electrostatic field is the same as in the plate-plate case, electrostatic transport is much less effective because turbulence intensity is higher where the electrostatic field is the weakest. The collection efficiencies are, in fact, lower.

Concentration profiles at various downstream locations are shown in Figure 13: all the profiles are well developed showing a central area of the duct being quickly depleted of particles, but still having characteristics typical of the phenomenon. Figure 14 compares computed concentration profiles against the data by Kihm. Data were obtained for boundary generated turbulence with a mean velocity of $2 \text{ m} \cdot \text{s}^{-1}$. The agreement of the data and the results is good.

Efficiencies were calculated and compared with the data, as shown in Figure 15 and Table 3. The experiments refer to turbulence generated by the shear with the wall and by baffles. Data referring to wall turbulence were obtained for a mean velocity of $2 \text{ m} \cdot \text{s}^{-1}$ and match accurately with the results obtained in this study, while the baffle-induced turbulence data obtained for a mean velocity of $1 \text{ m} \cdot \text{s}^{-1}$ show a lower efficiency due to the higher turbulent diffusion rate.
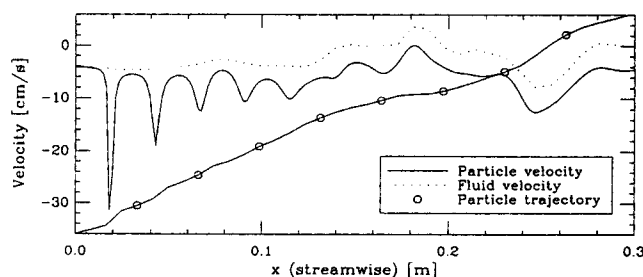

Figure 11. Plate-plate precipitator.

Efficiencies at different Deutsch numbers. Comparison of computed results (+) against data by Kihm (o , ◊) and Deutsch model (——).

Figure 12. Wire-plate precipitator.

Trajectory (⊖) of a particle, its velocity (——) and fluid velocity at particle location. The particle starts from the middle of the channel and deposits at the wall.
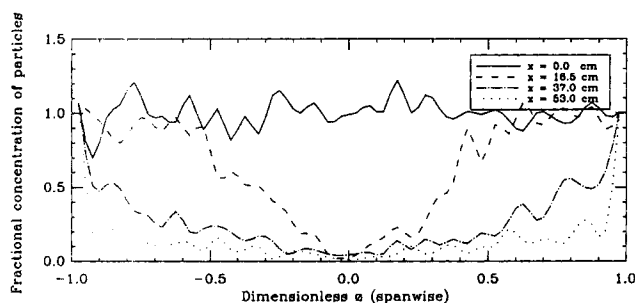
Figure 13. Wire-plate precipitator.

Evolution of particle fractional concentration profiles along the streamwise coordinate.

Figure 15. Wire-plate precipitator.

Efficiencies at different Deutsch numbers. Comparison of computed results (+) against data by Kihm (o , ◊) and Deutsch model (——).

Figure 16 shows the actual migration velocities referring to both the plate-plate and wire-plate cases. The actual migration velocity gives a measure of the mass transfer in the precipitator. The interpretation of experimentally measured "actual" migration velocity is not straightforward. Difficulties usually arise in discerning the effects of particle size distribution, particle charge, or flow conditions. However, the detailed nature of the information that can be obtained through the use of direct numerical simulation allows us to distinguish between the various effects that dominate particle migration. It is worth noting that the migration velocity is lower in the wire-plate geometry than in the plate-plate geometry, thus giving the overall lower efficiency.

Rather interestingly and in agreement with previous results (Robinson, 1967), the actual migration velocity decreases as particle collection proceeds for both precipitator geometries. We believe this decrease to be due to the characteristics of wall-generated turbulence. As deposition proceeds, particles tend to concentrate in the wall region rather than in the bulk flow. Therefore, as the turbulence intensity is higher in this region, particles are more affected by turbulent diffusion, which to first order is as likely to take them away from the wall as toward it than by the electrostatic drift, which tends to take them to the wall. The net effect is a decrease in migration velocity.

Summary and Conclusions

The technique of direct numerical simulation through the use of a pseudospectral method has been applied successfully
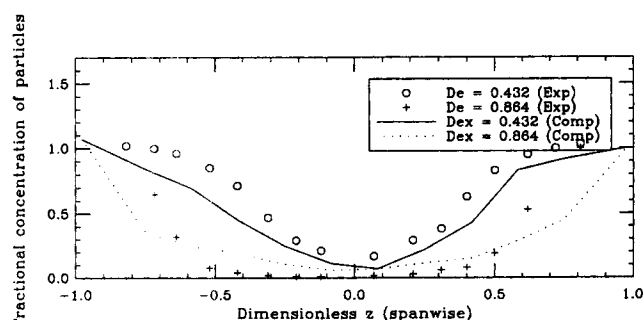

Figure 14. Wire-plate precipitator.

Particle fractional concentration at two different dimensionless coordinates (Deutsch numbers). Comparison of computed results (——, ·····) against data by Kihm (o , +).
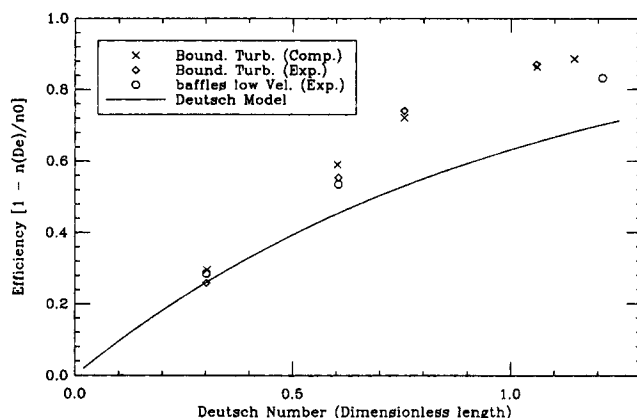
to simulate the transport of particles in turbulent flows under the action of different electrostatic fields. This represents the first attempt to apply this powerful and relatively new technique to solve problems of industrial interest, that is, electrostatic precipitation. The direct numerical simulation has been until now used to clarify turbulence mechanisms at fairly low Reynolds numbers, because the demands of computer time and computer memory are fairly high when it comes to solve high Reynolds number problems. On the other hand, the geometry and the flow parameters of electrostatic precipitators are such—the Reynolds numbers are low enough—that DNS can be used without insurmountable needs for computational resources. However, although the code is highly vectorialized, not parallelized, fast running code, the central processing unit (CPU) time required to perform one time step of the flow field simulation on a CRAY YMP supercomputer was slightly more than a second.

Aerosol particles have been followed in their motion in a numerically simulated turbulent flow field at a Reynolds number of about 6,000 and under the action of a uniform and constant electrostatic field characterizing a plate-plate electrostatic precipitator, and a highly nonuniform, but constant, electrostatic field characteristic of a wire-plate precipitator with no discharge occurring. Discharge-related phenomena, though important in electrostatic precipitation at higher field strengths, have not been accounted for in this article.

The turbulent flow field generated has been checked against experimental results, and the simulation is believed accurate. Particle transport data, directly obtained by solving the equation of motion of each particle, have been verified qualitatively

Table 3. Wire-Plate Precipitator Efficiencies

Deutsch No.	Deutsch Eff.	Exp.	Comp.
0.302	0.260	0.295*	0.295
0.302	0.260	0.286**	0.295
0.605	0.454	0.553*	0.591
0.605	0.454	0.535**	0.591
0.756	0.530	0.740*	0.720
1.058	0.653	0.970*	0.863

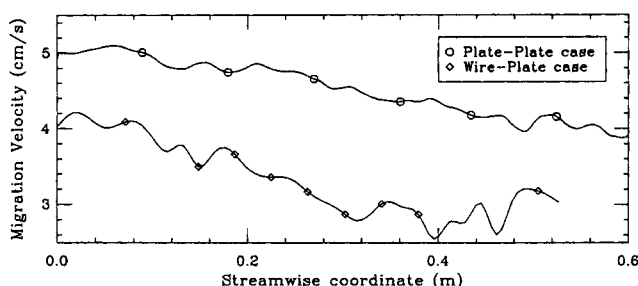* no baffles
** 1-cm single baffles

Figure 16. Actual migration velocity in plate-plate and wire-plate geometries.

Computed results at different streamwise coordinate values.

and quantitatively against experimental results obtained by Kihm (1987). The comparison with experimental data gives good agreement for both types of precipitators, suggesting that the technique employed is suitable for clarifying basic phenomena in electrostatic precipitation. This technique is capable of accurate analysis of phenomena not traceable elsewhere, as, for instance, in the determination of the actual migration velocity. The approach presented here is to develop more industrial codes that can be based, for instance, on the large eddy simulation (LES) technique, the basic philosophy of which is to explicitly compute only the large-scale motions, peculiar to the problem of interest being the smaller-scale motions more universal and therefore more easily described by simple models. Detailed information required to model subgrid-scale (SGS) effects, which are not resolved by LES, is made available by DNS.

Acknowledgment

Notation

d = precipitator characteristic width
d_p = particle diameter
De = Deutsch number
e = electrostatic field unity vector
E = electrostatic field
F = form factor
Fr_p = particle electrostatic Froude number
g = gravity vector
h = duct semiwidth
k_1 = wave number in the streamwise direction
k_2 = wave number in the spanwise (or vertical) direction
k_3 = wave number in the cross-stream direction
m = mass
n = number of particles
n_w = number of wires
p = pressure
q = electrostatic charge
r_c = dimensionless wire electrode radius
Re = Reynolds number
t = time
u = streamwise velocity component
U_m = mean velocity
v = spanwise velocity component
V = electrostatic potential
V_c = electrostatic potential applied at the wire electrode

w = cross-stream velocity component
w_e = migration velocity
x = streamwise coordinate
X_x = shape factor for the electrostatic field in the streamwise direction
X_z = shape factor for the electrostatic field in the cross-stream direction
y = spanwise (or vertical) coordinate
z = cross-stream coordinate

Greek letters

δ = dimensionless duct semiwidth
δ_{3i} = mean kinematic pressure gradient
ζ = dimensionless cross-stream coordinate
η = efficiency
μ = dynamic viscosity
ν = kinematic viscosity
ξ = dimensionless streamwise coordinate
ρ = density
τ_w = shear stress at the wall
τ_p = particle relaxation time

Subscripts

av = average
c = centerline
f = fluid
i, j = coordinate indices
m = mean
p = particle
x = streamwise coordinate
y = spanwise (or vertical) coordinate
z = cross-stream coordinate
τ = dimensionless in wall units
0 = inlet section

Superscripts

$\hat{}$ = Fourier transformed variable
$'$ = fluctuating velocity component

Literature Cited

Antonia, R. A., M. Teitel, J. Kim, and L. W. B. Browne, "Low-Reynolds Number Effects in a Fully Developed Turbulent Channel Flow," *J. Fluid Mech.*, **236**, 579 (1992).

Bohm, J., "Zur Frage des Rücksprühens bei der Elektrischen Gasreinigung," *Staub-Reinhalt. Luft*, **30**, 99 (1970).

Brodkey, R. S., J. M. Wallace, and H. Eckelmann, "Some Properties of Truncated Turbulence Signals in Bounded Shear Flows," *J. Fluid Mech.*, **63**, 209 (1974).

Castellanos, A., "Coulomb-Driven Convection in Electrohydrodynamics," *IEEE Trans. Electrical Insulation*, **26**, 1201 (1991).

Comte-Bellot, G., "Contribution a l'Étude de la Turbulence de Conduite," Thèse de Doctorat, Université de Grenoble, France (1963).

Deutsch, W., "Bewegung und Ladung der Elektricititatstrager in Zylinder Kondensator," *Ann. Phys.*, **58**, 335 (1922).

Eckelmann, H., "The Structure of Viscous Sublayer and the Adjacent Wall Region in a Turbulent Channel Flow," *J. Fluid Mech.*, **65**, 439 (1974).

Kallio, G. A., "Interaction of Electrostatic and Fluid Dynamic Fields in Wire-Plate Pecipitators," PhD Diss., Dept. of Mechanical and Material Engineering, Washington State Univ., Pullman (1987).

Kallio, G. A., and D. E. Stock, "Interaction of Electrostatic and Fluid Dynamic Fields in Wire-Plate Electrostatic Precipitators," *J. Fluid Mech.*, **240**, 133 (1992).

Kihm, K. D., "Effects of Nonuniformities on Particle Transport in Electrostatic Precipitators," PhD Diss., Dept. of Mechanical Engineering, Stanford Univ., Stanford, CA (1987).

Kim, J., P. Moin, and R. Moser, "The Turbulence Statistics in Fully Developed Channel Flow at Low Reynolds Number," *J. Fluid Mech.*, **177**, 133 (1987).

Kreplin, H. P., and H. Eckelmann, "Behaviour of the Three Fluc-

tuating Velocity Components in the Wall Region of a Turbulent Channel Flow," *Phys. Fluids*, **22**, 1233 (1979).

Lam, K., "Numerical Investigation of Turbulent Flow Bounded by a Wall and a Free-Slip Surface," PhD Diss., Dept. of Chemical and Nuclear Engineering, Univ. of California at Santa Barbara (1989).

Lam, K., and S. Banerjee, "On the Condition of Streak Formation in Bounded Flows," *Phys. Fluids A*, **4**, 306 (1992).

Leonard, G. L., M. Mitchner, and S. A. Self, "An Experimental Study of the Electrohydrodynamic Flow in Electrostatic Precipitators," *J. Fluid Mech.*, **127**, 123 (1983).

Leonard, G. L., M. Mitchner, and S. A. Self, "Particle Transport in Electrostatic Precipitators," *Atmospheric Environ.*, **14**, 1289 (1980).

Leonard, G. L., M. Mitchner, and S. A. Self, "Experimental Study of the Effect of Turbulent Diffusion on Precipitator Efficiency," *J. Aerosol. Sci.*, **13**, 271 (1982).

Maxey, M. R., and J. J. Riley, "Equation of Motion for a Small Rigid Sphere in a Nonuniform Flow," *Phys. Fluids*, **26**, 883 (1983).

McCluskey, F. M. J., and A. T. Perez, "The Electrohydrodynamic Plume Between a Line Source of Ions and a Flat Plate," *IEEE Trans. Elec. Ins.*, **27**, 334 (1992).

Riehle, C., and F. Löffler, "The Effective Migration Rate in Electrostatic Precipitators," *Aerosol Sci. Technol.*, **16**, 1 (1992).

Robinson, M. A., "Modified Deutsch Efficiency Equation for Electrostatic Precipitation," *Atmospheric Environ.*, **1**, 193 (1967).

Rowe, P. N., and G. A. Henwood, "Drag Forces in Hydraulic Model of a Fluidised Bed: I," *Trans. Instn. Chem. Engrs.*, **39**, 43 (1961).

Self, S. A., K. D. Kihm, and M. Mitchner, "Precipitator Performance Improvement through Turbulence Control," *Int. Conf. Electrostatic Precipitators*, Avano/Venice, Italy (1987).

Self, S. A., M. Mitchner, and K. D. Kihm, "Effects of Turbulence in Wire-Plate Precipitators," *EPA/EPRI Symp. on Particulate Control Technol.*, Nashville (1988).

Tennekes, H., and J. L. Lumley, *A First Course in Turbulence*, MIT Press, Cambridge, MA (1972).

Utami, T., and T. Ueno, "Experimental Study on the Coherent Structure of Turbulent Open-Channel Flow Using Visualization and Picture Processing," *J. Fluid Mech.*, **174**, 399 (1987).

Wallace, J. M., R. S. Brodkey, and H. Eckelmann, "The Wall Region in Turbulent Shear Flow," *J. Fluid Mech.*, **54**, 39 (1972).

Williams, J. C., and R. Jackson, "The Motion of Solid Particles in an Electrostatic Precipitator," *Cong. of the Europ. Fed. of Chem. Eng., Symp. Interaction Between Fluids and Particles*, p. 282 (1962).

Yamamoto, T., and H. R. Velkoff, "Electrohydrodynamics in an Electrostatic Precipitator," *J. Fluid. Mech.*, **108**, 1 (1981).

Appendix

Following Bohm (1970) the expression for the form factor is:

$$F = \ln\frac{4h}{\pi r_c} + \sum_{i=1,n_w} \frac{\cosh\left(\pi i \frac{\delta}{2}+1\right)}{\cosh\left(\pi i \frac{\delta}{2}-1\right)}$$

and the expressions for the field shape factors are:

$$X_\xi = \cos\frac{\pi}{2}\xi \left\{ \frac{\sinh\frac{\pi}{2}\zeta}{\cosh^2\frac{\pi}{2}\xi} - \cos^2\frac{\pi}{2}\zeta \right.$$

$$- \sum_{i=1,n_w} \frac{\sinh\frac{\pi}{2}(i\delta-\xi)}{\cosh^2\frac{\pi}{2}(i\delta-\xi) - \cos^2\frac{\pi}{2}\zeta}$$

$$\left. - \sum_{i=1,n_w} \frac{\sinh\frac{\pi}{2}(i\delta+\xi)}{\cosh^2\frac{\pi}{2}(i\delta+\xi) - \cos^2\frac{\pi}{2}\zeta} \right\}$$

$$X_\zeta = \sin\frac{\pi}{2}\xi \left\{ \frac{\cosh\frac{\pi}{2}\zeta}{\cosh^2\frac{\pi}{2}\xi} - \cos^2\frac{\pi}{2}\zeta \right.$$

$$- \sum_{i=1,n_w} \frac{\cosh\frac{\pi}{2}(i\delta-\xi)}{\cosh^2\frac{\pi}{2}(i\delta-\xi) - \cos^2\frac{\pi}{2}\zeta}$$

$$\left. - \sum_{i=1,n_w} \frac{\cosh\frac{\pi}{2}(i\delta-\xi)}{\cosh^2\frac{\pi}{2}(i\delta+\xi) - \cos^2\frac{\pi}{2}\zeta} \right\}$$

where the variables ξ and ζ are, respectively, the streamwise (x) and cross-stream (z) coordinates made dimensionless by the duct half-width, h, δ is the dimensionless duct half-width, and r_c is the dimensionless wire radius. The summations are extended over the total number of wires, n_w.